DWBA-WM DIFFERENTIAL CROSS SECTIONS FOR POSITRON IMPACT IONIZATION OF H_2

NEGAR ZOHOURI HAGHIAN

A THESIS SUBMITTED TO THE FACULTY OF GRADUATE STUDIES
IN PARTIAL FULFILMENT OF THE REQUIREMENTS
FOR THE DEGREE OF

MASTER OF SCIENCE

GRADUATE PROGRAM IN DEPARTMENT OF PHYSICS AND
ASTRONOMY
YORK UNIVERSITY
TORONTO, ONTARIO
JULY 2013

DWBA-WM DIFFERENTIAL CROSS SECTIONS FOR POSITRON IMPACT IONIZATION OF H_2

by **Negar Zohouri Haghian**

a thesis submitted to the Faculty of Graduate Studies of York University in partial fulfilment of the requirements for the degree of

MASTER OF SCIENCE

DWBA-WM DIFFERENTIAL CROSS SECTIONS FOR POSITRON IMPACT IONIZATION OF H_2

by **Negar Zohouri Haghian**

Examination Committee Members:

1. Dr. Radu I. Campeanu (Supervisor)
2. Dr. Al Stauffer
3. Dr. Jurij W. Darewych
4. Dr. Marin Litoiu

Abstract

The calculation of Triple differential cross sections (TDCS) using the Distorted Wave Born Approximation (DWBA) with the Ward and Macek (WM) approximation to post collision interaction is performed for positron impact ionization of molecular hydrogen. The purpose of this study is to examine whether the DWBA-WM model produces better results compared to the more elaborate 3C model. We performed two investigations. First, the DWBA-WM study of the phenomenon of electron capture to the continuum where we found that the DWBA-WM produces better agreement with experimental measurement than the 3C model for 50 eV positron projectiles. However for 100 eV positron impact energies, no theoretical model predicts correctly the variation of the TDCS with ejected electron energies. The second investigation was on the variation of the TDCS with non-zero scattering angles. We found that DWBA-WM produces very similar results to the 3C model except at the recoil peak. Since no experimental results are available, we cannot conclude which of the two methods produces more reliable results.

To my father, who wanted this more than anyone else.

Acknowledgements

I would like to thank those who have helped and inspired me during my graduate study at York University. I especially want to thank Dr. Radu Campeanu, my supervisor, for his guidance, continuous support and encouragement. He was always willing to help me with my research. Thank you for providing me with constructive comments and timely support during my thesis write up.

I would also like to thank the members of my supervisor committee, Dr. Al Stauffer and Dr. Jurij Darewych, for their guidance during my first year evaluation and defense. I appreciate their time and patients to read through my thesis and providing me with their valuable comments for better improvement of this work.

Special thanks goes to Mrs. Marlene Caplan for her kind assistance during the past two years.

Last but not least, I would like to thank my parents, my brother and my fiancé who have always been patient with me and supported me thought my battle with Crohn's disease. Without them this work would not have been possible.

Table of Contents

List of Tables

List of Figures

Abbreviations

3C	Three Coulomb Wavefunctions Model
3DW	Three Distorted Wave Model
a.u.	Atomic Units
CEM	Channel Electron Multiplier
DWBA	Distorted Wave Born Approximation
ECC	Electron Capture to the Continuum
FWHM	Full Width at Half Maximum
MCP	Michrochannel Plates
PCI	Post Collision Interaction
PPA	Parallel Plate Analyzer
TDCS	Triple Differential Cross Sections
WM	Ward and Macek Post Collision Interaction Approximation

1 Introduction

Triple Differential cross section (TDCS) measurements provide great insights into scattering collisions and motivate the development of sophisticated methods to study atomic systems in detail. The TDCS studies constitute a much better test on the theory than the integrated ionization cross section studies.

In the past two decades the theoretical treatment of TDCS for electron impact ionization of atoms showed impressive progress [9]. By comparison the positron impact ionization studies were very few and less sophisticated. The main problem was the availability of positron beams. Since the mono-energetic positron beams have low intensities, the experiments for the study of positron impact ionization are only relative. Thus the variation can be obtained, but not the absolute magnitude of the TDCS results.

The very first TDCS measurements on positron impact ionization of molecular hydrogen were designed to study the electron capture to the continuum. ECC is a special ionization case where the ejected electron is captured by the projectile

in a low lying continuum state. This phenomenon occurs due to the Coulomb attraction between the active electron and scattered projectile in the final state of the system [4]. If scattered positrons and ejected electrons emerge with the same energy in the same direction, they tend to stay together, forming a virtual positronium atom, which increases the collision cross section. Until recently, the ECC phenomenon was studied theoretically only with the 3C model, such as the studies by Fiol et al. [5] and Benedek et al. [6]. However, these papers showed that for very low impact energies the 3C models fail to agree with the experiment.

In a recent investigation, Campeanu [10] included the post collision interaction (PCI) approximation of Ward and Macek in the Distorted Wave Born Approximation (DWBA) model. DWBA is a relatively simple method, representing the final state of the system as a product of two wavefunctions representing the scattered positron and ejected electron. The DWBA-WM model was employed to study the ECC phenomenon in positron impact ionization of helium [10]. Campeanu was able to show that in the case of He targets, the DWBA-WM model produced results that were in better agreement with the ECC experimental data than the more elaborate 3C model of Benedek et al [6]. Therefore the question was raised as to whether the same is true in the case of ECC studies of molecular hydrogen.

The purpose of this work is to compare the DWBA-WM model to the 3C model of Benedek et al. [6, 8] in a further examination of positron impact ionization of

H_2. This work consists of two separate studies in order to achieve this objective. First, the DWBA-WM is applied in the study of ECC phenomenon where the scattered positron and ejected electron are at zero degree scattering angle. The TDCS results are then compared to the 3C results of Benedek et al. [6]. Second, the effect of variation of the TDCS with non-zero scattering angles are investigated by comparing the two models. Unfortunately for this study, there are no experimental data available yet.

This work is organized in the following manner. Chapter 2 presents the experiments performed in the ECC study of positron impact TDCS measurements for molecular hydrogen. Chapter 3 will provide a general formulation of the theoretical calculations. This includes the provision of the primary definition of the cross section and T-matrix. As mentioned earlier, 3C was the first model used in the ECC study of H_2. Therefore in section 3.1 a short description of the theory and the formalism of the final state wavefunction are provided. Section 3.2 contains the DWBA model in its standard form where an expansion in partial waves and detailed expansion of the direct T-matrix is provided. In section 3.3 we provide a more detailed explanation of the DWBA-WM model in terms of a post collision interaction approximation. The distortion of positron and electron wavefunctions in various fields are described in details in section 3.4. Then in section 3.5, the numerical methods employed in performing the TDCS calculations are provided.

Chapter 4 consist of the results of our work. In section 4.1 the TDCS results of the electron capture to the continuum study are presented and section 4.2 includes the TDCS results obtained in the study of the variation with non-zero scattering angles. Finally in Chapter 5 the conclusions of our work are presented.

2 Experiments

In this chapter, we present the experimental method for obtaining TDCS for positron impact ionization of molecular hydrogen. For this target, the only TDCS measurements dealt with the study of the ECC phenomenon.

The early experiments studying the ECC phenomenon were carried out on proton-atom collisions and other heavier ion impacts in the 1960s and 70s [11]. The results showed the presence of a cusp-like peak of the projectile in the electron energy spectrum, observed at 0° relative to the direction of the incident proton [1, 11]. This cusp-like peak was explained as a result of the Coulomb attraction between the ejected electron and scattered projectile in the final state of the system. The interaction started as the bound electron was ionized by the projectile. The attractive potential between the projectile and active electron caused the ionized electron to accelerate and be captured to a low lying continuum state known as ECC phenomenon.

Since the discovery of positrons, investigators were concerned about how antimatter-

matter interactions are different or similar to matter-matter interaction. In the early 1990s, researchers attempt to study the ECC phenomenon using positron impact. First, Double Differential Cross Sections (DDCS) – the already developed method of approximation used for the matter-matter interaction – failed to produce any significant results in identifying the ECC phenomenon [12]. Using heavy projectiles, the ECC was observed at zero angle, since the projectile is hardly deflected by the collision. In contrast, due to the nature of light projectiles, positrons are easily deflected. Thus the probability of ionization is very small at specific angles since they are spread over a large range [13]. Consequently, a higher degree of differential calculation is required to obtain a closer approximation. Hence, Triple Differential Cross Section (TDCS) of measurements were implemented both theoretically and experimentally; which provided detailed information about the dynamics of ionizing collisions.

The very first TDCS measurements on positron impact ionization of molecular hydrogen were conducted by Kövér and Laricchia of the University College Londen Positron Group in 1998 [1]. This experiment was designed to study the ECC phenomenon at $100\,eV$ impact energy. Hence the ejected electron emerged in the same direction at 0° as the scattered positron. In this experiment, the positron beam was created by a radioactive source, which provided a beam of 2×10^4 e^+ per second. This intensity was 10^{-9} less than the intensity used in electron impact

ionization. The positron beam was electrostatically guided. The experiment was

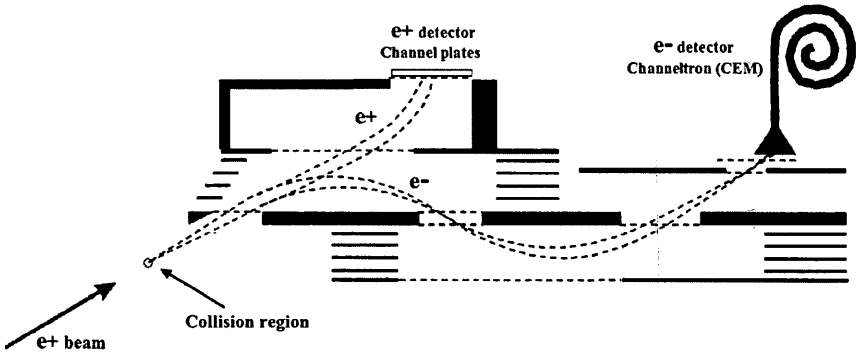

Figure 2.1: Schematic diagram of the 1998 experimental setup [1]

performed using a Channeltron (CEM) as illustrated in figure 2.1, where ejected electrons were detected. A tandem Parallel Plate Analyzer (PPA) determined the energy of the ejected electrons. Microchannel Plates (MCP) fixed on top of the first PPA were used to detect the scattered positrons. The angular acceptance of the electron detector in this experiment was approximately Gaussian shaped. The full width at half maximum (FWHM) angles were estimated in different directions as given in table 2.1. Furthermore, the energy resolution of the PPA was determined mainly by the size of the projectile beam and estimated to be about 10%. The experiment at $100\,eV$ positron impact energy was carried out for ejected electron energies of $15 - 55\,eV$ at $5\,eV$ intervals. At each energy, it took approximately $5 \times 10^5 s$ to obtain the data. A small broad peak was observed at $42\,eV$, which is

Table 2.1: The angular acceptance of e^- and e^+ detectors in the 1998 experiment [1]

	Azimuthal	Polar
Electron Detector	$\pm 4°$	$\pm 15°$
Positron Detector	$\pm 15°$	$+20°/-10°$

an indication of ECC phenomenon. As one can analyze,

$$42\,eV \approx \frac{100\,eV - 15.42\,eV}{2} \tag{2.1}$$

where $100\,eV$ is the projectile's impact energy and $15.42\,eV$ is the first ionization energy of H_2. This finding in 1998 was the very first experimental confirmation of ECC phenomenon for positron impact.

In 2001, a new experiment was conducted by the same group on $50\,eV$ positron impact ionization of H_2 [2]. The only change in the experimental apparatus was the use of a more advanced PPA as illustrated in figure 2.2. Due to its time focusing properties, the new PPA was able to direct electrons from different angles to reach the detector, all at the same time. Since at low energy, the signal to background ratios are higher, the new PPA was able to yield narrower time peaks. Other than the new PPA and the lower positron intensity beam, the coincident circuit and data collection procedure were the same as the 1998 experiment. The angular acceptance for the electron detector in this experiment was approximately

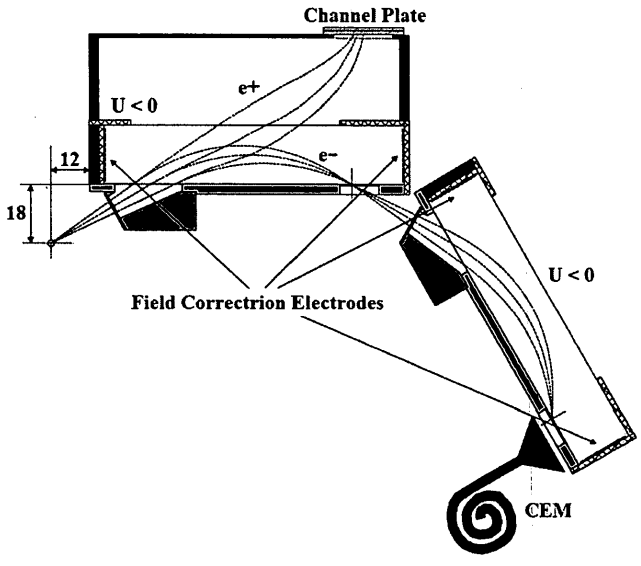

Figure 2.2: Schematic diagram of the 2001 experimental setup [3]

Gaussian shaped. The full width at half maximum (FWHM) angles were estimated in different directions as given in table 2.2. The energy resolution of the PPA was again approximately 10%. The experiment was carried out for ejected electron energies of $9 - 19\ eV$. The measuring time at each energy was again $5 \times 10^5\ s$ similar to the previous experiment. Fiol et al [5] calculated the theoretical peak of

Table 2.2: The angular acceptance of e^- and e^+ detectors in the 2001 experiment [2]

	Azimuthal	Polar
Electron Detector	±4°	±15°
Positron Detector	±18°	±18°

the cross section as

$$17.3\,eV \approx \frac{50\,eV - 15.42\,eV}{2}. \tag{2.2}$$

When this value was convoluted according to the experimental angular and energy resolution, the theoretical peak was shifted to $16.5\,eV$ [5]. However, the experimental peak was observed at around $15\,eV$ and this showed a shift by $2.3\,eV$ toward lower ejected electron energies. Kövér et al explained that an error in the calibration of the experimental energy is unlikely, yet not entirely excluded, and suggested the shift was due to a possible physical effect, for instance, energy loss during ionization as a result of vibrational excitation or molecular dissociation of the target. However, the shift should have been $1.33\,eV$ and not $2.3\,eV$, if ECC lead to dissociation of the residual ion;

$$1.33\,eV \approx \frac{2.65\,eV}{2} \tag{2.3}$$

where $2.65\,eV$ is the dissociation energy of H_2^+.

A new study by Arcidiacono et al [4] from the same UCL group was conducted in 2005. The energy spectrum of positrons scattered from H_2 was detected for the first time. The goal was to further investigate whether molecular dissociation or vibrational excitation were responsible for the observed shift in the study by Kövér et al of 2001. In order to study molecular dissociation, the charge to mass ratio of the ion in the final state was calculated. Figure 2.3 illustrates the interacting region

for the triple coincidence system between scattered positron, ejected electron and residual ion. Once an electron with a particular energy was detected, the system was triggered to extract the ions that were in the scattering region. The target gas chosen was Deuterium D_2, which is one of the stable isotopes of hydrogen. The purpose of choosing D_2 was to distinguish between the ion from other background gases and to increase the lifetime of the ion in the extraction region. Detection

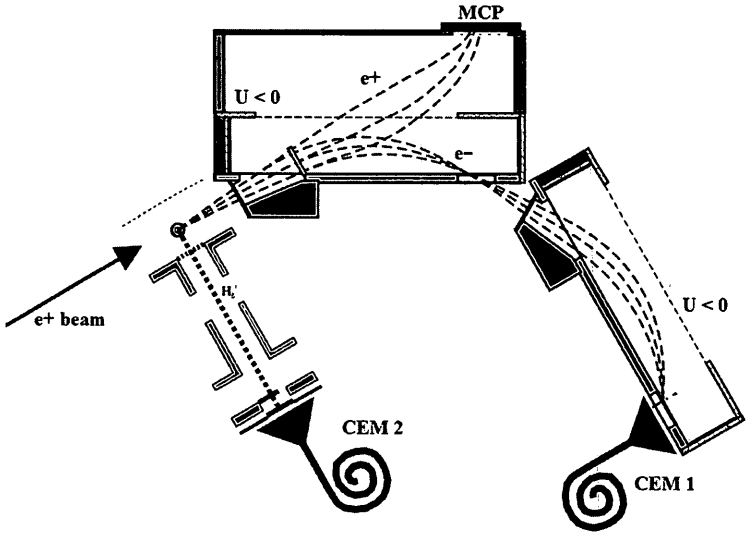

Figure 2.3: Schematic diagram of the 2005 experimental setup [4]

of the electron and ion pair then triggered the initiation of another measurement, which stopped when a positron was detected. The charge to mass ratio of the ion was finally determined based on the time of flight spectrum. This spectrum was obtained from the delayed coincidence between the two channel electron multipliers CEM1 and CEM2. In this study, two concluding remarks were made regarding the

study in 2001 [3]:

1. Based on two grounds, the shift observed is not due to dissociative ionization, since no D^+ was present. Also the TDCS energy dependency in this experiment was the same as previously observed in 2001.

2. The shift observed is not due to energy loss of the target, i.e. molecular excitation. The energy distributions of scattered positrons and ejected electron are closely related by:

$$E_+ = E_i - E_- - I \tag{2.4}$$

where I is the ionization energy, E_+ is the energy of the scattered positron, E_i is the energy of the incoming positron and E_- is the energy of the ejected electron, which demonstrate the conservation of energy.

Arcidiacono et al were able to observe asymmetries in energy sharing between the two leptons. The asymmetries were observed at approximately half the residual energy. The positron spectrum was shifted to higher energies by $1.5\,eV$ and the electron spectrum was shifted by the same amount to lower energies [4]. A contributing factor might be the low velocities of these particles in the final state of the system. However, since there is no quantum mechanical theory that could fully explain this behaviour, the data are appropriate for use in testing various approaches.

3 Theory

The Triple Differential Cross Section (TDCS) in general has the form,

$$\sigma^{(3)} = \frac{\mathrm{d}^3\sigma}{\mathrm{d}\Omega_f \, \mathrm{d}\Omega_e \, \mathrm{d}E_e} = N_{i,e,f,b} \times |T|^2, \tag{3.1}$$

where T is the T-matrix representing the transition amplitude for ionization and N is a normalization factor, described in more details in equation (3.12). The index i represents the incident positron, e denotes the ejected electron, f stands for the scattered positron and b is the bound electron. The ejected electron energy is denoted as E_e, and $\mathrm{d}\Omega_f$, $\mathrm{d}\Omega_e$ are the elements of solid angles representing the direction of the scattered positron and ejected electron.

The exact T-matrix has the form [14],

$$T = \langle \widetilde{\Psi}_f | V | \Psi_i \rangle, \tag{3.2}$$

where the perturbation is $V = (H - H_0)$. In this equation, H is the full Hamiltonian of the system and H_0 represents the approximate Hamiltonian of the initial state.

Also, $\widetilde{\Psi}_f$ and Ψ_i are the eigenfunctions of the two Hamiltonians,

$$H_0 |\Psi_i\rangle = E |\Psi_i\rangle \quad \text{and} \quad H |\widetilde{\Psi}_f\rangle = E |\widetilde{\Psi}_f\rangle. \tag{3.3}$$

In the case of electron impact ionization, the T-matrix includes both the direct and exchange Coulomb matrix elements. In the case of positron impact ionization there is no exchange between the ejected electron and scattered positron in the final channel. Thus throughout this thesis T will be equal to the direct transition matrix.

In this study, atomic units ($\hbar = e = m_e = 1$) are used.

3.1 3C Model

TDCS for positron impact ionization of H_2 were calculated using 3C models by Brauner et al. [15], Fiol et al. [5] and Benedek et al. [6]. In these models, the initial state of the system is represented as a product of the free positron wavefunction in the field of H_2 multiplied by the electron hydrogenic bound state wavefunction, while the final state of the system is represented as a product of three continuum Coulomb wavefunctions, a Coulomb wave for each of the ejected electron and the scattered positron in the field of the residual H_2^+ and another Coulomb wave for the interaction between the two leptons.

For this three body problem it is convenient to use the Jacobi coordinates as shown in figure 3.1. In this system, the position coordinates of each body is replaced by a relative position $\mathbf{r}_j$ between two bodies, and a vector to their centre of mass $\mathbf{R}_j$. Similarly $\mathbf{k}_j$ and $\mathbf{K}_j$ are the related terms in momentum space, where j denotes any of T, N or P.

$\mathbf{r}_T$: position vector of the ejected electron relative to residual ion target T

$\mathbf{r}_P$: position vector of the ejected electron relative to the projectile P

$\mathbf{r}_N$: position vector of the projectile relative to T

$\mathbf{R}_T$: vector from the centre-of-mass of e and T relative to P

$\mathbf{R}_N$: vector from the centre-of-mass of T and P relative to e

$\mathbf{R}_P$: vector from the centre-of-mass of e and P relative to T

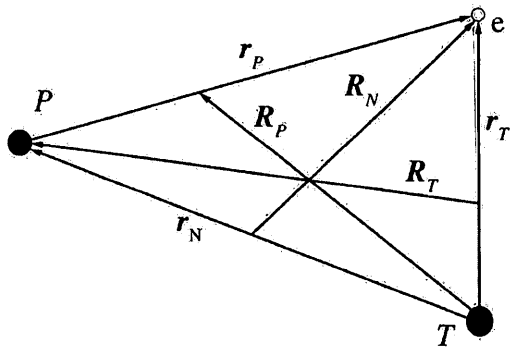

Figure 3.1: Jacobi coordinates for the three-body problem

Using these coordinates, the 3C model initial state wavefunction will be

$$\Psi_i = \frac{e^{i\mathbf{K}_T^i \cdot \mathbf{R}_T}}{(2\pi)^{3/2}} \phi_i(\mathbf{r}_T) \tag{3.4}$$

where ϕ_i is the initial bound state, represented by a hydrogenic $1s$ type wavefunction

$$\phi_i(r_T) = \frac{\beta^{(3/2)}}{\sqrt{\pi}} e^{-\beta r_T}. \tag{3.5}$$

The effective charge of the residual target β is given by the binding energy of the electron in the molecule

$$\beta = (2m_T\varepsilon_i)^{1/2}. \tag{3.6}$$

In 3C model the final state wavefunction according to Fiol et al. [5] can be approximated as,

$$\Psi_f^-(\mathbf{r}_j, \mathbf{R}_j) = \frac{e^{i(\mathbf{k}_j \cdot \mathbf{r}_j + \mathbf{K}_j \cdot \mathbf{R}_j)}}{(2\pi)^3} D^-(\nu_T, \mathbf{k}_T, \mathbf{r}_T) D^-(\nu_P, \mathbf{k}_P, \mathbf{r}_P) D^-(\nu_N, \mathbf{k}_N, \mathbf{r}_N). \tag{3.7}$$

In this equation, D^- represent the distortion factors defined in terms of two body Coulomb wavefunctions,

$$\psi^-_{\mathbf{k}_j}(\mathbf{r}_j) = (2\pi)^{-3/2} e^{i\mathbf{k}_j \cdot \mathbf{r}_j} D^-(\nu_j, \mathbf{k}_j, \mathbf{r}_j). \tag{3.8}$$

Hence the distortion factor for a continuum state with Coulomb interactions is denoted as,

$$D^-(\nu_j, \mathbf{k}_j, \mathbf{r}_j) = N^-(\nu_j)\, {}_1F_1(i\nu_j; 1; -i(k_j r_j + \mathbf{k}_j \mathbf{r}_j)). \tag{3.9}$$

In this equation, ${}_1F_1$ is the confluent hypergeometric function given by Abramowitz et al. [16], $N^-(\nu_j)$ is,

$$N^-(\nu_j) = \Gamma(1 - i\nu_j) e^{-\pi\nu_j/2}, \tag{3.10}$$

and the Sommerfeld parameter ν_j is given by,

$$\nu_j = \frac{m_j Z_j}{k_j}. \tag{3.11}$$

The 3C approximation assumes complete overlap of the H_2 and H_2^+ wavefunctions. This is why the residual H_2^+ wavefunction does not appear in this theory.

In the 3C approach, the nine-fold integral appearing in the transition matrix can be reduced to a six dimensional integral. In order to evaluate this numerically, Nordsieck [17] integrals were used to further reduce it to a three dimensional integral. Even so, the numerical integration in the 3C model presents many challenges [18], since the positron and electron Coulomb waves are not independent and

angular decomposition is not possible, which is the main disadvantage of using the 3C model to evaluate the TDCS. Another drawback is the fact that the distorting effects of the target on the projectile is completely ignored in this model.

3.2 DWBA Model

In the Distorted Wave Born Approximation (DWBA) model, the positron and the active electron (i.e. the electron which is ejected) are considered independent from each other. This allows each lepton wavefunction to be decomposed into angular and radial parts. The advantage with the DWBA is the fact that by using polar coordinates the angular integrations can be done analytically. Therefore the 6-fold integration over the polar coordinates become a 2-fold integration over the two radial coordinates.

We calculated the triple differential cross section for positron impact ionization of molecular hydrogen according to Kheifets et al. [19],

$$\frac{\mathrm{d}^3\sigma}{\mathrm{d}\Omega_f\,\mathrm{d}\Omega_e\,\mathrm{d}E_e} = 2\,(2\pi)^4\,\frac{k_e k_f}{k_i}\int |T(\mathbf{k}_i,\mathbf{k}_e,\mathbf{k}_f)|^2\,\mathrm{d}\Omega_{\boldsymbol{\rho}_0}, \tag{3.12}$$

where $\boldsymbol{\rho}_0$ represents the internuclear equilibrium vector over the orientation of which one has to average the cross section and $\mathbf{k}_i, \mathbf{k}_e, \mathbf{k}_f$ denote the momentum of the incident positron, ejected electron and scattered positron respectively. In order to take into account the existence of two electrons in molecular hydrogen, a factor of 2 is multiplied at the beginning of the equation. In our work the integral over the orientation of the internuclear equilibrium vector was performed when we calculated the spherically integrated representation of the molecular hydrogen wave function and static potential.

In atomic units, wave vectors and momenta are equal, hence in this study we used wave vectors in the calculation of the T-matrix.

Generally, wavefunctions can be decomposed into radial and angular parts,

$$\Psi(\mathbf{r}) = \frac{1}{r} R_{nl}(r) Y_{lm}(\hat{\mathbf{r}}), \tag{3.13}$$

where n, l and m are the principal quantum number, angular momentum and magnetic quantum number respectively and Y_{lm} are spherical harmonics. For continuum state wavefunctions the decomposition is more complicated. The positron wavefunctions for the positron initial and final states are:

$$\Phi_i(\mathbf{r}_1) = \sum_{l_i} (-i)^{l_i} e^{-i\delta_{l_i}} R_{l_i}(k_i, r_1) \sum_{m_i} Y^*_{l_i m_i}(\hat{\mathbf{r}}_1) Y_{l_i m_i}(\hat{\mathbf{k}}_i) \tag{3.14}$$

$$\Phi^*_f(\mathbf{r}_1) = \sum_{l_f} i^{l_f} e^{i\delta_{l_f}} R_{l_f}(k_f, r_1) \sum_{m_f} Y_{l_f m_f}(\hat{\mathbf{r}}_1) Y^*_{l_f m_f}(\hat{\mathbf{k}}_f) \tag{3.15}$$

The active electron wavefunctions for the electron initial and final state are:

$$\Phi_b(\mathbf{r}_2) = \Phi_b(r_2) Y_{l_b m_b}(\hat{\mathbf{r}}_2). \tag{3.16}$$

$$\Phi^*_e(\mathbf{r}_2) = \sum_{l_e} i^{l_e} e^{i\delta_{l_e}} R_{l_e}(k_e, r_2) \sum_{m_e} Y_{l_e m_e}(\hat{\mathbf{r}}_2) Y^*_{l_e m_e}(\hat{\mathbf{k}}_e) \tag{3.17}$$

In these equations, $\mathbf{r}_1$ denotes the positron's position vector and $\mathbf{r}_2$ denotes the positron of active electron. Φ_i and Φ_f are the initial and final state of the positron projectile, whereas Φ_e and Φ_b are the wavefunction of the ejected electron and bound electron respectively.

The radial wavefunction R_{l_j} were obtained as solutions of the Schrödinger equation by

$$R_{l_j}(r) = \sqrt{\frac{2}{\pi}}\,\frac{1}{kr}\,y_{l_j}(r), \tag{3.18}$$

where j denotes one of i, f, b or e [20] and $y_{l_j}(r)$ are the functions that satisfy the Schrödinger equation,

$$\left[\frac{\mathrm{d}^2}{\mathrm{d}r^2} - \frac{l(l+1)}{r^2} - 2V_j(r) + k^2\right] y l_j(k, r) = 0. \tag{3.19}$$

In this equation, V_j stands for the different potentials as described in section 3.4. According to Kheifets et al. [19] the T-matrix element of equation (3.12) can be written as,

$$\begin{aligned} T &= \langle \Phi_f(\mathbf{r}_1)\,\Phi_e(\mathbf{r}_2) \mid V \mid \Phi_i(\mathbf{r}_1)\,\Phi_b(\mathbf{r}_2) \rangle\,, \\ &= \int\int \mathrm{d}\mathbf{r}_1\,\mathrm{d}\mathbf{r}_2\,\Phi_f^*(\mathbf{r}_1)\,\Phi_e^*(\mathbf{r}_2)\,V\,\Phi_b(\mathbf{r}_2)\,\Phi_i(\mathbf{r}_1). \end{aligned} \tag{3.20}$$

The DWBA approximation assumes complete overlap of the H_2 and H_2^+ wavefunctions. This is why the residual H_2^+ wavefunction containing the coordinates of the second molecular electron does not appear in our theory. The potential V corresponds to the interaction between the positron projectile and the target components.

According to Kheifets et al. [19] in the DWBA approximation, the expression of V is reduced to the interaction between the positron and the active electron, which

can be expanded in a series according to Levine [21],

$$V = \frac{1}{|\mathbf{r}_1 - \mathbf{r}_2|} = \sum_{\lambda,\mu} \frac{4\pi}{2\lambda+1} \frac{r_<^\lambda}{r_>^{\lambda+1}} Y^*_{\lambda\mu}(\hat{\mathbf{r}}_1)\, Y_{\lambda\mu}(\hat{\mathbf{r}}_2), \tag{3.21}$$

where $r_<$ denotes the smaller of r_1 and r_2, $r_>$ denotes the larger of the two.

Inserting the expression for V and the wavefunctions given in (3.14–3.17) into (3.20), we obtain the following expression for the T-matrix element,

$$\begin{aligned} T = \int\int \mathrm{d}\mathbf{r}_1\, \mathrm{d}\mathbf{r}_2 \Bigg[& \left(\sum_{l_f} i^{l_f} e^{i\delta_{l_f}} R_{l_f}(k_f, r_1) \sum_{m_f} Y^*_{l_f m_f}(\hat{\mathbf{r}}_1) Y_{l_f m_f}(\hat{\mathbf{k}}_f) \right) \\ & \left(\sum_{l_e} i^{l_e} e^{i\delta_{l_e}} R_{l_e}(k_e, r_2) \sum_{m_e} Y^*_{l_e m_e}(\hat{\mathbf{r}}_2) Y_{l_e m_e}(\hat{\mathbf{k}}_e) \right) \left(\sum_{\lambda,\mu} \frac{4\pi}{2\lambda+1} \frac{r_<^\lambda}{r_>^{\lambda+1}} Y_{\lambda\mu}(\hat{\mathbf{r}}_1)\, Y^*_{\lambda\mu}(\hat{\mathbf{r}}_2) \right) \\ & \left(\Phi_b(r_2) Y_{l_b m_b}(\hat{\mathbf{r}}_2) \right) \left(\sum_{l_i} (-i)^{l_i} e^{-i\delta_{l_i}} R_{l_i}(k_i, r_1) \sum_{m_i} Y_{l_i m_i}(\hat{\mathbf{r}}_1) Y^*_{l_i m_i}(\hat{\mathbf{k}}_i) \right) \Bigg] \end{aligned} \tag{3.22}$$

The T-matrix element can be evaluated using Clebsch-Gordan coefficients or equivalently the Wigner 3-j symbols,

$$\langle j_1 m_1\, j_2 m_2 | j_3 m_3 \rangle = C^{j_3 m_3}_{j_1 m_1 j_2 m_2} = (-1)^{m_3 + j_1 - j_2} \sqrt{2j_3 + 1} \begin{pmatrix} j_1 & j_2 & j_3 \\ m_1 & m_2 & -m_3 \end{pmatrix}. \tag{3.23}$$

The angular integrations in equation (3.22) are product of three spherical harmonics. For positron angles, they are:

$$\int Y^*_{l_f m_f}(\hat{\mathbf{r}}_1) Y_{\lambda\mu}(\hat{\mathbf{r}}_1) Y_{l_i m_i}(\hat{\mathbf{r}}_1)\, \mathrm{d}\hat{\mathbf{r}}_1. \tag{3.24}$$

The angular integrations over the active electron are:

$$\int Y^*_{l_e m_e}(\hat{\mathbf{r}}_2) Y^*_{\lambda\mu}(\hat{\mathbf{r}}_2) Y_{l_b m_b}(\hat{\mathbf{r}}_2)\, \mathrm{d}\hat{\mathbf{r}}_2. \tag{3.25}$$

These integrals are shown by Varshalovich et al. [22] to give products of Clebsch-Gordan coefficients.

To simplify further, we chose the z-axis along the direction of $\mathbf{k}_i$, which means the $\theta_i = 0$ thus,

$$Y_{l_i m_i}(\hat{\mathbf{k}}_i) = \sqrt{\frac{(2l_i+1)}{4\pi}}\delta_{m_i,0}. \tag{3.26}$$

Since the conservation law is valid for the angular momentum in the z-component, we know the 3-j symbols must be zero unless $m_b + \mu = m_e$ and $m_f + \mu = m_i$, so $m_f + m_e = m_i + m_b$. Since hydrogen is in a $1s$ orbital, $l_b = 0$ and $m_b = 0$; we also know $m_i = 0$ from equation (3.26).

Following these operations, the T-matrix element is:

$$\begin{aligned} T = & \sum_{\substack{l_i l_e l_f \lambda \\ m_i m_e m_f \mu}} e^{i(\delta_{l_i}+\delta_{l_e}+\delta_{l_f})} i^{(l_i-l_e-l_f)}(-1)^{m_e} \\ & \times \begin{pmatrix} l_f & \lambda & l_i \\ -m_f & m_f & 0 \end{pmatrix} \begin{pmatrix} l_f & \lambda & l_i \\ 0 & 0 & 0 \end{pmatrix} \begin{pmatrix} l_b & \lambda & l_e \\ -m_b & m_f & m_e \end{pmatrix} \begin{pmatrix} l_b & \lambda & l_e \\ 0 & 0 & 0 \end{pmatrix} \\ & \times \sqrt{\frac{(2l_i+1)}{4\pi}}\, Y_{l_f m_f}(\hat{\mathbf{k}}_f)\, Y_{l_e m_e}(\hat{\mathbf{k}}_e) \sqrt{(2l_i+1)(2l_e+1)(2l_f+1)(2l_b+1)} \\ & \int_0^\infty \mathrm{d}r_1 \int_0^\infty \mathrm{d}r_2\, r_1^2\, r_2^2\, R_{l_f}(k_f, r_1)\, R_{l_e}(k_e, r_2)\, \frac{r_<^\lambda}{r_>^{\lambda+1}}\, R_{l_b}(r_2) R_{l_i}(k_i, r_1) \end{aligned} \tag{3.27}$$

Alternatively the T-matrix can be written in terms of a reduced Coulomb matrix

element:

$$\langle k_f k_e \| V \| k_i b \rangle = \sqrt{(2l_i+1)(2l_e+1)(2l_f+1)(2l_b+1)} \times \begin{pmatrix} l_f & \lambda & l_i \\ 0 & 0 & 0 \end{pmatrix} \begin{pmatrix} l_b & \lambda & l_e \\ 0 & 0 & 0 \end{pmatrix} R^{\lambda}_{l_i l_e l_f l_b}(k_i, k_e, k_f, n_b), \tag{3.28}$$

where the last term is a Slater integral given as,

$$\int_0^\infty \mathrm{d}r_1 \int_0^\infty \mathrm{d}r_2 \, r_1^2 \, r_2^2 \, R_{l_f}(k_f, r_1) \, R_{l_e}(k_e, r_2) \, \frac{r_<^\lambda}{r_>^{\lambda+1}} \, \Phi_b(r_2) \, R_{l_i}(k_i, r_1). \tag{3.29}$$

The radial functions $R_{l_f}(k_f, r_1)$, $R_{l_e}(k_e, r_2)$, $R_{l_i}(k_i, r_1)$ were evaluated using the Schrödinger equation for the potentials as explained in section 3.4. Also, Φ_b represents the spherically averaged wavefunction of molecular hydrogen using the Wang approximation,

$$\Phi_b(r_2) = \frac{1}{4\pi} \int \Phi_{Wang}(\mathbf{r}_2, \mathbf{r}_3) \, \mathrm{d}\mathbf{r}_3 \, \mathrm{d}\hat{r}_2, \tag{3.30}$$

where Φ_{Wang} is given by Wang in 1928 [23] and $\mathbf{r}_3$ represents the position vector of the second bound electron. Investigations by Campeanu et al. [24], using this wavefunction have shown it produces good results for integrated ionization cross section.

Using a Slater integral has the advantage of having radial variables separated from the angular part. Therefore the radial integration can be done analytically and the result would multiply each term of the sum.

The T-matrix element in equation (3.27) was then simplified to,

$$T = \sum_{\substack{l_i l_e l_f \lambda \\ m_e m_f}} e^{i(\delta_{l_i}+\delta_{l_e}+\delta_{l_f})} i^{(l_i-l_e-l_f)} (-1)^{m_e} \sqrt{\frac{(2l_i+1)}{4\pi}}\, Y_{l_f m_f}(\hat{\mathbf{k}}_f) Y_{l_e m_e}(\hat{\mathbf{k}}_e)$$
$$\times \begin{pmatrix} l_f & \lambda & l_i \\ -m_f & m_f & 0 \end{pmatrix} \begin{pmatrix} l_b & \lambda & l_e \\ -m_b & m_f & m_e \end{pmatrix} \langle k_f k_e \| V \| k_i b \rangle. \tag{3.31}$$

3.3 DWBA-WM Model

The standard DWBA model represents the final state of the system as a product of two wavefunctions, one for the scattered projectile and another for the ejected electron. The Coulomb interaction between the two leptons is not taken into consideration in the standard model. We now turn to modifications which are required to allow for post collision interaction (PCI) in the final state of the system.

Brauner et al. [15] were able to show improvements in theoretical results when PCI was included in the final state wavefunction as opposite to including PCI as a perturbation. The reason lies with the fact that any physics contained in the wavefunction would be included in all orders of perturbation, while including the PCI in the potential is only applied to the first order of perturbation theory.

Investigators have previously suggested the use of the Gamow factor along with a hypergeometric function to account for the Coulomb interaction between the two leptons in the final state of the system. In a study by Botero and Macek [25], the DWBA-G model was suggested as a way to improve theoretical results by using a Gamow factor and neglecting the hypergeometric function. However, in a later study by Ward and Macek [26], the use of a low energy approximation of the hypergeometric function was suggested to account for the average separation between the ejected electron and scattered projectile.

This model was called DWBA-WM and produced very good results when applied by Madison and Al-Hagan [14] in a study of electron impact ionization TDCS. Recently, Campeanu [10] applied the same model in the study of positron impact ionization of helium and obtained good agreement with experimental data of Kövér et al. [2]. In this study we use the Ward and Macek approximation to account for post collision interaction.

The external factor in the Ward and Macek approximation of PCI between the ejected electron and scattered positron is,

$$|C_{scat-eject}|^2 = G \left| {}_1F_1\left(\frac{i\gamma}{2\pi}, 1, \frac{i2\pi}{\gamma} r_{ab}^{ave}\right)\right|^2, \tag{3.32}$$

where

$$\begin{aligned} G &= \frac{\gamma}{\exp(\gamma) - 1}, \\ \gamma &= \frac{-\pi}{|\mathbf{k}_f - \mathbf{k}_e|}. \end{aligned} \tag{3.33}$$

The third parameter of the hypergeometric function can be represented as,

$$r_{ab}^{ave} = \frac{\pi^2}{16\,\varepsilon_t}\left(1 + \frac{0.627}{\pi}\sqrt{\varepsilon_t}\,\ln\varepsilon_t\right)^2, \tag{3.34}$$

where ε_t represents the total energy of ejected electron and scattered positron.

3.4 Distorted Waves used in DWBA-WM

In our study of positron impact ionization of H_2 using the DWBA-WM model, we included the distortion of both positron and ejected electron wavefunctions in various fields.

In the initial state, the incident positron is distorted due to the static field of the molecular hydrogen. The static field can be calculated by,

$$V_{st}(r_1) = V_{nucl}(r_1) - \frac{2}{r_1}\int_0^{r_1} \Phi_b^2(x)\,\mathrm{d}x - 2\int_{r_1}^{r_1 max} \Phi_b^2(x)\frac{1}{x}\,\mathrm{d}x. \tag{3.35}$$

In this formula, the second and third terms represent the attraction potential between the positron and the two bound state electrons. The centre of the molecule is considered to be at 0 and r_1 is the position of the positron. In this equation r_{1max} is the value of which this molecular wavefunction becomes zero numerically. Also, $\Phi_b^2(r_2)$ represents the radial charge density of the bound state electron in H_2 molecule.

The term $V_{nucl}(r_1)$ in equation (3.35) is given according to the "shell model" introduced by Al-Hagan et al. [27] as,

$$V_{nucl}(r_1) = \begin{cases} \dfrac{2}{r_1} & if\ r_1 \geq 0.7 a.u. \\ 0 & if\ r_1 < 0.7 a.u. \end{cases} \tag{3.36}$$

$V_{nucl}(r_1)$ is a repulsive potential between the positron and the two nuclei of the molecular hydrogen. We did not consider the target polarized by the incident

positron.

In the final state channel, there are three cases to be considered depending on the energy of the scattered positron as compared to the energy of the ejected electron.

- **Case 1: scattered positron is faster than ejected electron ($\mathbf{k}_f > \mathbf{k}_e$)**

  In this situation, as the scattered positron looks back, it "sees" that the ejected electron and the residual ion form a virtual hydrogen molecule. Thus the scattered positron observes a potential that is similar to the potential of the incident channel.

  In the ejected electron channel on the other hand, we used the Coulomb potential of H_2^+ ion and the Furness-McCarthy exchange potential between the bound and ejected electrons,

$$V_{ex}(r_2) = -\frac{1}{2}\left\{\left(E_e - \frac{1}{r_2}\right) - \sqrt{\left(E_e - \frac{1}{r_2}\right)^2 - 2\,\Phi_b^2(r_2)}\right\}, \qquad (3.37)$$

  where the exchange potential is considered to be singlet. Table 3.1 includes the potentials employed in Case 1.

- **Case 2: ejected electron is faster than scattered positron ($\mathbf{k}_e > \mathbf{k}_f$)**

  In this case, the ejected electron is moving much faster so as it looks back, it observes two positive charges. Thus simple Coulomb potential and the Furness-McCarthy exchange are applied to the ejected electron channel.

Table 3.1: The potentials in the final state channel when ($\mathbf{k}_f > \mathbf{k}_e$), ($\mathbf{k}_e > \mathbf{k}_f$) or ($\mathbf{k}_f = \mathbf{k}_e$)

Associated Potentials		**Case 1**	**Case 2**	**Case 3**
Incident e^+	Φ_i	$V_{st}(r_1)$	$V_{st}(r_1)$	$V_{st}(r_1)$
Scattered e^+	Φ_f	$V_{st}(r_1)$	$\frac{1}{r_1}$	$\frac{1}{r_1}$
Ejected e^-	Φ_e	$-\frac{1}{r_2} + V_{ex}(r_2)$	$-\frac{2}{r_2} + V_{ex}(r_2)$	$-\frac{1}{r_2} + V_{ex}(r_2)$

In the scattered positron channel, only a simple Coulomb potential is used. The reason is when the scattered positron looks back, it only observes a single positive charge. Table 3.1 includes the potentials employed in Case 2.

- **Case 3: ejected electron and scattered positron have the same energy ($\mathbf{k}_e = \mathbf{k}_f$)**

  In this situation, both outgoing leptons "see" the positive charge of the residual molecular ion. The potentials used in this case are given in table 3.1.

3.5 Numerical Methods

Radial Schrödinger Equation

The radial solutions to the Schrödinger equations given by equation (3.19) were numerically calculated with the NUMEROV subroutine developed in the 1970s by the theoretical atomic physics group at University College London [28]. The radial integration of the three continuum wavefunctions provided the radial wavefunctions for the incident positron, the scattered positron and the ejected electron. These equations were solved on an equidistant mesh going from origin, where the nucleus was positioned. We used a mesh with the step 0.035 a.u. extended outward to about 10 a.u., which was well into the asymptotic range of the three continuum wavefunctions. The NUMEROV routine was able to detect the start of the asymptotic regions. NUMEROV routine solves the equations for both Coulomb and non-Coulomb potentials.

Radial Integration

The double radial integrals of the DWBA model were evaluated by using the composite Simpson integration method. As the integrand was a function of both r_1 and r_2, before doing the external Simpson summation, we "froze" the r_1 and performed the internal Simpson's summation for r_2. Then our program performed the external

Simpson summation for r_1.

Convolution Integral

In order to compare our theoretical results to experimental values in case of ECC phenomenon, we performed the convolution of the theoretical TDCS with the finite resolution of the experimental angular and energy values. The finite acceptance of the experiment by the UCL Positron Group [1, 2, 4] are given in table 2.1 and table 2.2. There were one energy and four angular experimental inaccuracies, therefore we had a 5 fold convolution integrals.

We applied the convolution as follows:

$$\frac{\mathrm{d}^3\sigma}{\mathrm{d}\Omega_f\,\mathrm{d}\Omega_e\,\mathrm{d}E_e} = \int \frac{\mathrm{d}^3\sigma}{\mathrm{d}\Omega_f\,\mathrm{d}\Omega_e\,\mathrm{d}E_e}(x)\; g(x)\,\mathrm{d}x, \tag{3.38}$$

where $g(x)$ represents the normal (Gaussian) distribution [29], given by

$$g(x) = \left[\frac{1}{\sigma\sqrt{2\pi}}\, exp\left(\frac{-(x-\mu)^2}{2\sigma^2}\right)\right]. \tag{3.39}$$

For each experimental inaccuracy, there were several possible values, thus it was convenient to assume that there is a normal distribution of the measured values.

Our normal distribution function had a negative exponential factor. Therefore we solved the integration by using Gauss-Hermite quadrature [30], which has a similar form

$$\int_{-\infty}^{+\infty} e^{-x'^2} f(x')\,\mathrm{d}x' \approx \sum_{i=1}^{n} w_i f(x'_i). \tag{3.40}$$

Using the Gauss-Hermite quadrature implies the change of variable:

$$x = x' \sqrt{2}\, \sigma + \mu \tag{3.41}$$

everywhere in the TDCS calculation.

In equation (3.40), n denotes the number of sample points used in the approximation. The convolution was performed by using a $(n = 5)$ point Gauss-Hermite quadrature for each of these experimental inaccuracies. We checked the variation of TDCS values with the number of Gaussian points (we tried 3, 5 and 7 points) and found that the 5 points quadrature is sufficiently accurate. The roots of the Hermite polynomials $H_n(x')$ are denoted as x'_i where $(i = 1, ..., n)$ and w_i are the associated weights given by,

$$w_i = \frac{n!\, 2^{n-1}\sqrt{\pi}}{n^2 (H_{n-1}(x'_i))^2}. \tag{3.42}$$

For instance, the width σ for θ_e was 4°. The convolution for θ_e where $\mu = 0$ was approximated by changing equation (3.41) to:

$$x = x' \sqrt{2}\, \sigma \tag{3.43}$$

where $\sigma = 4 \left(\frac{\pi}{180}\right)$ radians.

Partial Wave Expansion

Finally we have to mention that the expansion with partial waves was truncated. The effect of truncation was a small error, approximately 10^{-3} in our results. This

value was obtained by increasing the number of partial waves until the change in the results was small error of 10^{-3}. The convergence with partial waves was achieved by using a maximum of 40 partial waves in the incident and scattered positron continuum states. We also use a maximum of 10 partial waves in the ejected electron channel. In all cases, the values were obtained by running the program several times with different input values to find the number of partial wave that converged the results.

4 Results and Discussion

This chapter consists of the TDCS results obtained by applying our DWBA-WM model to positron impact ionization of molecular hydrogen. In section 4.1, the DWBA-WM model was applied to both low and high positron impact energies of 50 eV and 100 eV in order to study the ECC phenomenon at zero scattering and ejection angles. The results were then compared to the positron and electron 3C models of Benedek et al. [6] and Fiol et al. [5]. In section 4.2, the variation of scattering angles in determining the TDCS is considered. Our DWBA-WM model is applied to 100 eV and 250 eV impact energies, both at a small ejected electron energy of 4.5 eV at various scattering angles. This is followed by the comparison of our data with the positron and electron 3C models of Benedek et al. [8] and Stia et al. [7]. In this study, the TDCS values are in atomic units and energies are in electron volts.

4.1 Results for Electron Capture to the Continuum

In our ECC study of positron impact ionization of molecular hydrogen, a cylindrical symmetry was used where the scattered positron and the ejected electron emerged in the forward direction. Although the experiment was attempting to detect both leptons at zero degree scattering angles, due to experimental uncertainties, the symmetry of the experiment could not be coplanar. In this study we used the associated potentials of **Case 3** as explained in section 3.4.

Using the DWBA-WM model we calculated the TDCS values at 50 eV impact energy with various ejected electron energies E_e. We found the ECC peak to be where the scattered positron and ejected electron had the same energy of 17.3 eV. The TDCS values obtained for 50 eV impact are present in table 4.1. In order to compare our theoretical data to the experimental values obtained by Kövér et al. [1], convolution with the experimental angular and energy resolution of table 2.1 are required. Therefore, five experimental uncertainties were included in our study. Table 4.2 provides the details on one energy and four angular corrections.

After the convolution was applied, we observed two important changes to our results. First, the TDCS values obtained in table 4.1 were significantly reduced in size. Second, the ECC peak previously observed at 17.3 eV in the unconvoluted calculation was shifted to a lower ejected electron energy of 15 eV. The asymmetry

Table 4.1: DWBA-WM unconvoluted TDCS values for 50 eV impact ionization of H_2 at zero scattered and ejected angles

E_e (eV)	TDCS (a.u.)
9	1123.33
10	1075.94
11	1156.41
12	1287.86
13	1389.88
14	1589.36
15	2015.56
16	2776.16
17	5339.54
18	4055.31
19	654.79
20	312.56
21	182.87

of our data is responsible for the shift of the ECC peak. The change in unconvoluted TDCS results at ejected electron energies lower than the ECC peak ($E_e < 17.3\,eV$) is not as rapid as the change of TDCS values after the ECC peak ($E_e > 17.3\,eV$). For instance in table 4.1, the change of TDCS values from $E_e = 11eV$ to $E_e = 12eV$ or from $E_e = 13eV$ to $E_e = 14eV$ are of the order of 100 $a.u.$. However this change after the ECC peak is of the order of 4000 $a.u.$ for $E_e = 18\,eV$ to $E_e = 19\,eV$.

The plot of the convoluted theoretical data associated with the unconvoluted data of table 4.1 is given in figure 4.1. Our DWBA-WM model predicted the ECC

Table 4.2: The ECC experimental uncertainties of H_2 positron impact [1]

	Symbol	Uncertainties
Ejected Electron Energy	E_e	$\pm 10\%$
Ejected Electron θ	θ_e	$\pm 4°$
Scattered Positron θ	θ_f	$\pm 15°$
Ejected Electron ϕ	ϕ_e	$\pm 15°$
Scattered Positron ϕ	ϕ_f	$+20°/-10°$

peak at 15 eV ejected electron energy, which is in agreement with the relative experimental data of Kövér et al. [1, 2]. However, the 3C models of Fiol et al. [5] and Benedek et al. [6] predicted the ECC peak at an ejection electron energy higher than the experimental energy by 1.6 eV.

Also the TDCS shape of our DWBA-WM model is in better agreement with the TDCS experimental shape when compared to the results of the 3C models of Fiol et al. [5] and Benedek et al. [6].

Another difference between the 3C model and our DWBA-WM model is the TDCS size. The experimental triangles on the graph were previously raised by Benedek et al. [18] to match the height of their ECC peak. In order to perform a clear comparison of the theoretical models, we multiplied our DWBA-WM curve by a factor of 2.5 as presented in figure 4.1. Since the experimental values were

obtained on a relative scale, it is not possible to conclude which theoretical model is able to obtain the correct result in terms of the TDCS size.

Benedek et al. [6] attribute the disagreement between their 3C model and experiment to the fact that the 3C model is missing the interaction between the direct ionization and the positronium formation channels [18]. Our DWBA-WM model only considers the direct ionization and is able to produce the correct position of the ECC peak relative to the experimental data.

Using the DWBA-WM model we repeated our calculation of the TDCS values at 100 eV impact energy with various ejected electron energies E_e. This time we found the ECC peak to be where the scattered positron and ejected electron had the same energy of 42.3 eV. The TDCS values obtained for 100 eV impact are presented in table 4.3. Again, convolution with experimental angular and energy resolution of table 4.2 was applied. The plot of the convoluted theoretical data associated with the unconvoluted data of table 4.3 is given in figure 4.2.

As shown, for 100 eV impact energy both the DWBA-WM and 3C models were able to produce the ECC peak at the experimental peak position at 43 eV ejected electron energy. Again, in order to allow for a clear comparison of the theoretical models we multiplied our DWBA-WM curve by a factor of 3.5. As in the 50 eV case, the experimental data of Kövér et al. [1, 2] were normalized to the 3C model results of Benedek at al. [6]. Figure 4.2 shows that for 100 eV positrons the EEC

Table 4.3: DWBA-WM unconvoluted TDCS values for 100 eV impact ionization of H_2 at zero scattered and ejected angles

$E_e(eV)$	TDCS (a.u.)
33	291.28
34	300.09
35	316.69
36	339.85
37	371.19
38	418.96
39	500.17
40	648.33
41	963.86
42	2083.72
43	3311.81
44	589.85
45	305.12
46	197.00

peak is predicted correctly by all theoretical models. However, at energies lower than $E_e = 40\,eV$ all three theoretical models disagree with each other and with the experimental values.

4.2 Results for the Variation of the TDCS with Scattering Angles

In this section we present the TDCS measurements for positron impact ionization of H_2 for various scattering angles. To discuss the ionization dynamics, our DWBA-WM model is compared to both the TDCS results of the electron 3C model of Stia et al. [7] and positron 3C model of Benedek et al. [8]. This study is performed for non-zero angles at two different impact energies of 100 eV and 250 eV in a coplanar symmetric geometry.

In case of electron impact ionization of molecular hydrogen, several experiments have been performed for different energies at various angles. However, there are no experimental results available in the case of positron impact for comparison. The TDCS electron 3C model of Stia et al. [7] produced theoretical results in great agreement with the absolute electron experimental results of Jung et al. [31] for all energies and angles. We compared our positron DWBA-WM theoretical data to the two 3C models of Benedek et al. [8] and Stia et al. [7] as shown in figure 4.3 and 4.4. We employed the DWBA-WM model and obtained the TDCS values for 100 eV positron impact energy at small scattering angles of 7° and 15°. The TDCS were calculated for 4.5 eV ejected electron energy and were presented as function of ejected electron angles. In both cases, the convergence of our DWBA-WM positron

curve to the 3C curve of Benedek et al. [8] was achieved by using 7 partial waves in the ejected electron channel and 30 in the incident positron channel. Our results were divided by a factor of 32.7 and 34.6 respectively to match the height of the 3C binary peak.

We performed the same study in case of 250 eV positron impact energy, for three different scattering angles of $\theta_f = 4°, 8°, 12°$. In all three variations of θ_f we used 10 partial waves in the ejected electron channel and 40 partial waves in the incident positron channel. In order to compare our results to the 3C model of Benedek et al. [8], we normalized our DWBA-WM binary peak to the magnitude of the 3C model binary peak by dividing our data by a factor of 26.3.

Generally, all curves show two maxima; one is referred to as the binary peak and the other as the recoil peak. Brauner et al. [15] describe the mechanism for electron impact ionization as following. The binary peak is the result of an electron-electron collision with the nucleus as a spectator. This peak is located approximately in the direction of the momentum transfer vector $\mathbf{q} = \mathbf{k}_i - \mathbf{k}_e$. The recoil peak is located approximately in the opposite direction to the binary peak. As a result of double scattering, the initially bound electron is scattered from the projectile electron and then scattered an infinite number of times off the target nucleus.

Figures 4.3 - 4.7 show the variation of the TDCS with scattering angles is quit similar when calculated with our DWBA-WM model and with the positron

3C model of Benedek et al. [8]. The only significant differences are in the recoil peak magnitude and position. This was expected as the recoil peak is due to the electron double scattering phenomenon, which depends on the representation of the PCI and of the electron wavefunctions in the field of the target. These two theoretical components were different in the DWBA-WM and 3C models.

In the remainder of this chapter, we shall focus on the comparison between our DWBA-WM results and the electron 3C results of Stia et al. [7]. As shown in figures 4.3 - 4.7, we observed a large difference between the size of our positron DWBA-WM binary peak as compared to that of the electron 3C binary peaks. For instance, at 100 eV impact energy and $\theta_f = 7°$, the positron binary peak is approximately 13 $a.u.$ larger than the electron binary peak. At $\theta_f = 15°$, the positron binary peak is 4 $a.u.$ larger. In case of 250 eV impact, at $\theta_f = 4°, 8°, 12°$, the positron binary peaks are about 8.4, 3.4 and 1.6 $a.u.$ larger than the electron binary peaks. Table 4.4 contains these differences. Thus an interesting feature observed in this study is that in all five cases, the positron binary peak is much larger compared to that of the electron peak. This is in agreement with the positron results of Berakdar [32] and Benedek et al. [8].

In studying the recoil peaks however, the electron 3C model of Stia et al. had slightly larger TDCS values as compared to our positron DWBA-WM results. At 100 eV impact energy, this difference is about 0.6 $a.u.$ in the case of $\theta_f = 7°$ and

0.2 $a.u.$ in the case of $\theta_f = 15°$. At 250 eV impact energy for scattering angles of $\theta_f = 8°, 12°$, the electron recoil peaks were 0.04 $a.u.$ and 0.03 $a.u.$ larger than our positron results. Figure 4.5 represents the 250 eV impact at $\theta_f = 4°$ scattering

Table 4.4: TDCS difference in sizes of the DWBA-WM e^+ to 3C e^- peaks

		Difference in Binary Peak	Difference in Recoil Peak
100 eV	7°	12.68 $a.u.$	- 0.58 $a.u.$
	15°	4.00 $a.u.$	- 0.19 $a.u.$
250 eV	4°	8.38 $a.u.$	+ 0.91 $a.u.$
	8°	3.42 $a.u.$	- 0.04 $a.u.$
	12°	1.63 $a.u.$	- 0.03 $a.u.$

angle. This was the only case where we did not have the electron recoil peak larger than the positron peak as shown in table 4.4.

This table compares the result of the TDCS in both cases of 100 eV and 250 eV impact where similar behaviour was observed. In all five cases, as the scattering angle was increased from 7° to 15° at 100 eV and from 4° to 12° at 250 eV, the differences in the TDCS values of both binary and recoil peak decreased dramatically in size. The same is true of the impact energy. As the impact energy was increased, the TDCS results were decreased.

As one replaces positrons with electron projectiles, two main features are observed. First, using a classical view, it can be argued that there is a higher proba-

bility for binary collisions to occur in case of the positron projectiles. This is due to the attraction force between the positron and the ejected electron, which pulls the ejected electron into the binary peak region. However, in case of electron projectiles, the repulsion between the two electrons pushes the ejected electron away and into the recoil region.

Table 4.5: The binary peaks positions of the three models relative to the direction of momentum transfer

			Binary Peak Positions		
		Direction of Momentum Transfer ($\mathbf{q} + 180°$)	Positron DWBA-WM	Positron 3C Model	Electron 3C Model
100 eV	7°	316°	318°	325°	300°
	15°	300°	302°	309°	288°
250 eV	4°	303°	309°	309°	296°
	8°	290°	289°	297°	285°
	12°	287°	290°	292°	282°

Second, changing the electron projectile to a positron projectile will have an affect on the bending of the binary and recoil peaks. Table 4.5 shows the momentum transfer in degrees for different impact energies and scattering angles. It also provides the binary peak positions of our positron DWBA-WM curves in comparison to both the electron and the position 3C models. We observed that our positron binary peaks are positioned on one side of the momentum transfer; whereas the

electron binary peaks are located on the opposite side. Thus the two projectile are bending in opposite directions as compared to the momentum transfer vector. This bending feature of the binary peak is noticeable when the scattering angle is relatively small. For instance when the impact energy is 250 eV and the $\theta_f = 4°$, our positron DWBA-WM curve is bent toward higher ejected electron angles by 6°. The electron 3C model curve on the other hand is bent toward the lower ejected electron angles by 7°. Thus, the positron binary peak is bending toward the forward direction and the electron binary peak bends toward the backward direction.

The opposite is true in case of the recoil peaks. From the five figures 4.3 - 4.7, except figure 4.5, we observed that in contrast to the binary peak, our recoil positron peaks are bent toward the backward direction and the electron recoil peaks are bent toward the forward direction. In figure 4.5 however, the direction of the momentum transfer is at $\mathbf{q} = 123°$, our DWBA-WM recoil peak is at 126° and the electron 3C peak is at 137°.

The shift of both binary and recoil peaks relative to the direction of the momentum transfer is due to the PCI effect and the distortion of the partial waves. Many studies have considered the effect of PCI in electron impact [33] and positron impact [34] ionization.

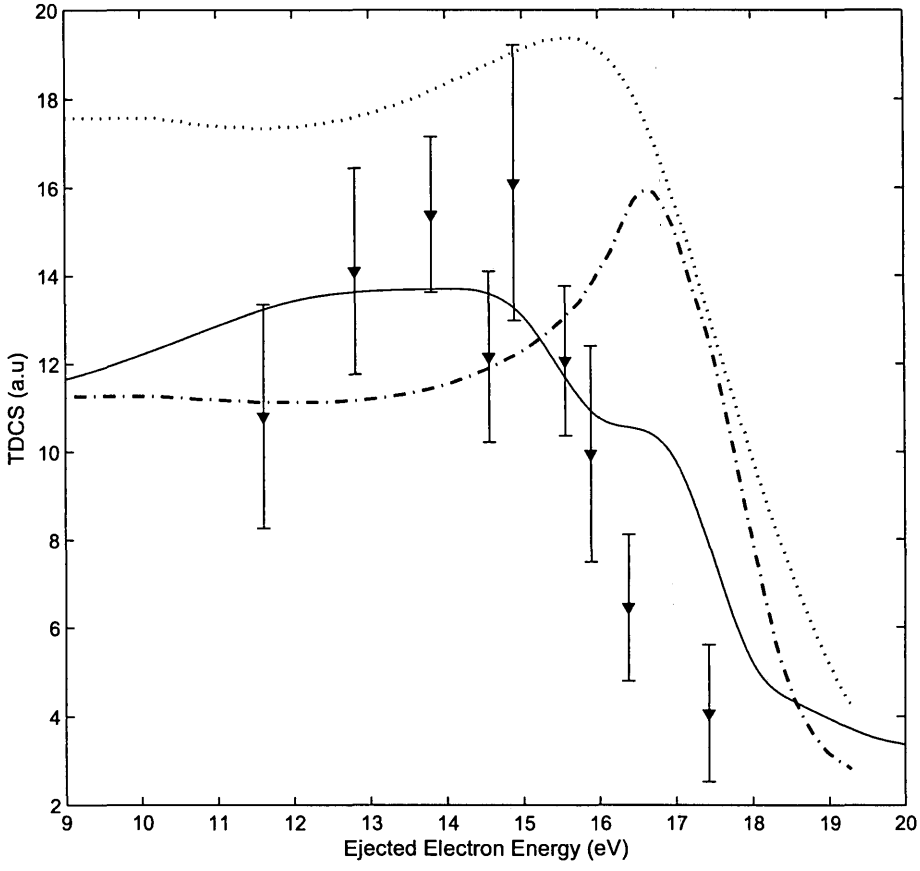

Figure 4.1: ECC study of $50eV$ positron impact ionization of molecular hydrogen. The TDCS $(a.u.)$ is convoluted with experimental angular and energy resolutions as function of ejected electron energy (eV). Our DWBA-WM model is represented by the solid curve, the 3C model of Fiol et al [5] by the dotted curve, the 3C model of Benedek et al [6] by dotted-dash curve and the experimental data of Kövér et al [1, 2] are represented by triangles and error bars. The experimental data were normalized to the height of the ECC peak by Benedek et al [6]. Our data was multiplied by a factor of 2.5.

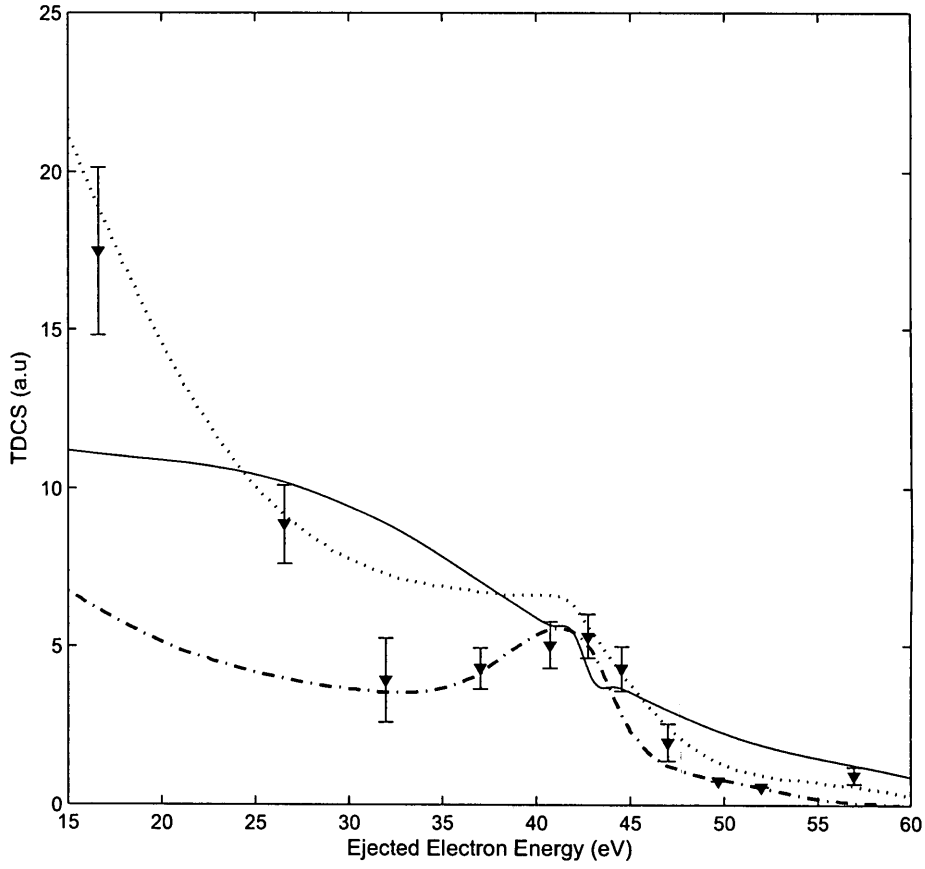

Figure 4.2: ECC study of 100 eV positron impact ionization of molecular hydrogen. The convoluted TDCS ($a.u.$) is a function of ejected electron energy (eV). Our DWBA-WM model is represented by the solid curve, the 3C model of Fiol et al. [5] by the dotted curve and the 3C model of Benedek et al. [6] by dotted-dash curve. The experimental data of Kövér et al. [1, 2] are represented by triangles and error bars, normalized to the height of the ECC peak by Benedek et al. [6]. Our data was multiplied by a factor of 3.5.

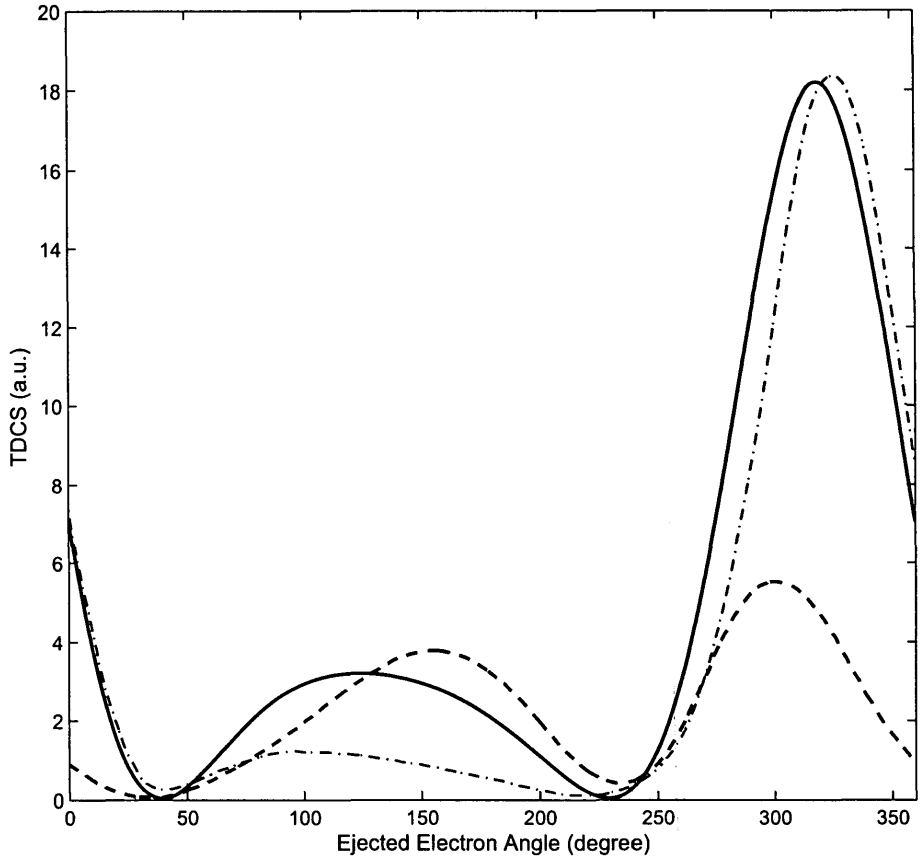

Figure 4.3: Angular dependent TDCS ($a.u.$) in coplanar asymmetric geometry at $E_i = 100\ eV$ positron impact energy, $E_e = 4.5\ eV$ ejection electron energy and $\theta_f = 7°$ scattering angle. Our positron DWBA-WM model is represented by the solid curve, the electron 3C model of Stia et al. [7] by the dashed curve and the positron 3C model of Benedek et al. [8] by the dotted-dash curve. In this study, 30 partial waves were used in the incident positron channel. The direction of the momentum transfer vector is at $\mathbf{q} = 136°$ and at $(\mathbf{q} + 180°) = 316°$. Our data was divided by a factor of 32.7.

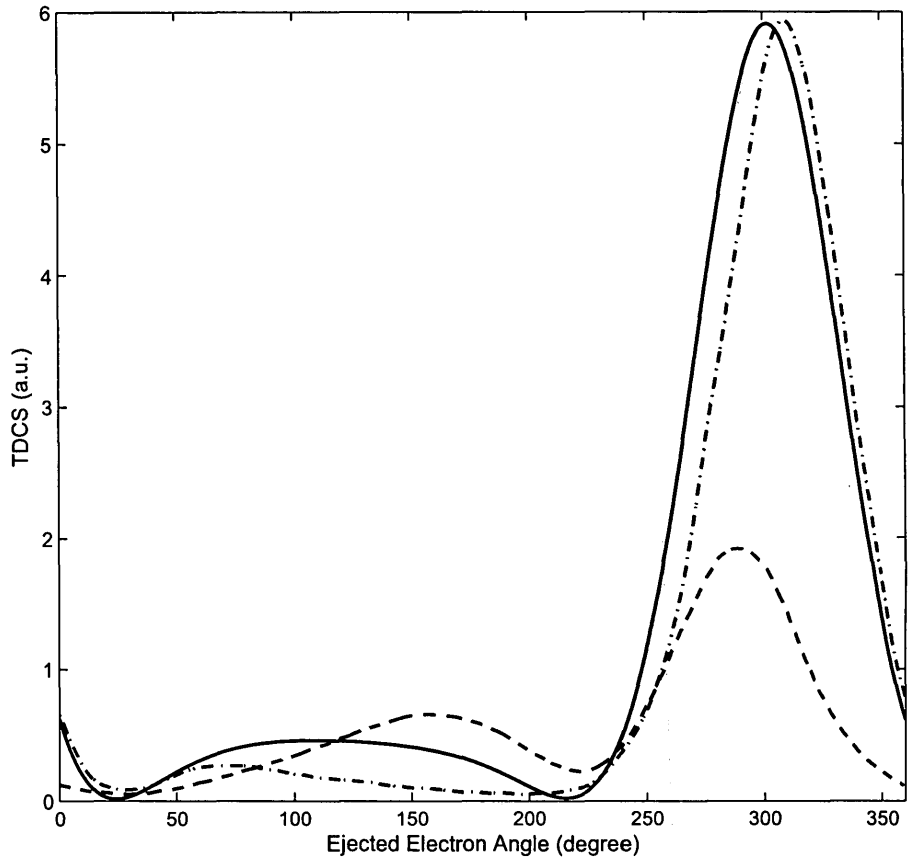

Figure 4.4: Angular dependent TDCS ($a.u.$) in coplanar asymmetric geometry at $E_i = 100\ eV$ positron impact energy, $E_e = 4.5\ eV$ ejection electron energy and $\theta_f = 15°$ scattering angle. Our DWBA-WM model is represented by the solid curve, the 3C electron impact of Stia et al. [7] by the dashed curve and the 3C positron impact of Benedek et al. [8] by the dotted-dash curve. The direction of the momentum transfer vector is at $\mathbf{q} = 120°$ and $(\mathbf{q} + 180°) = 300°$. Our data was divided by a factor of 34.6.

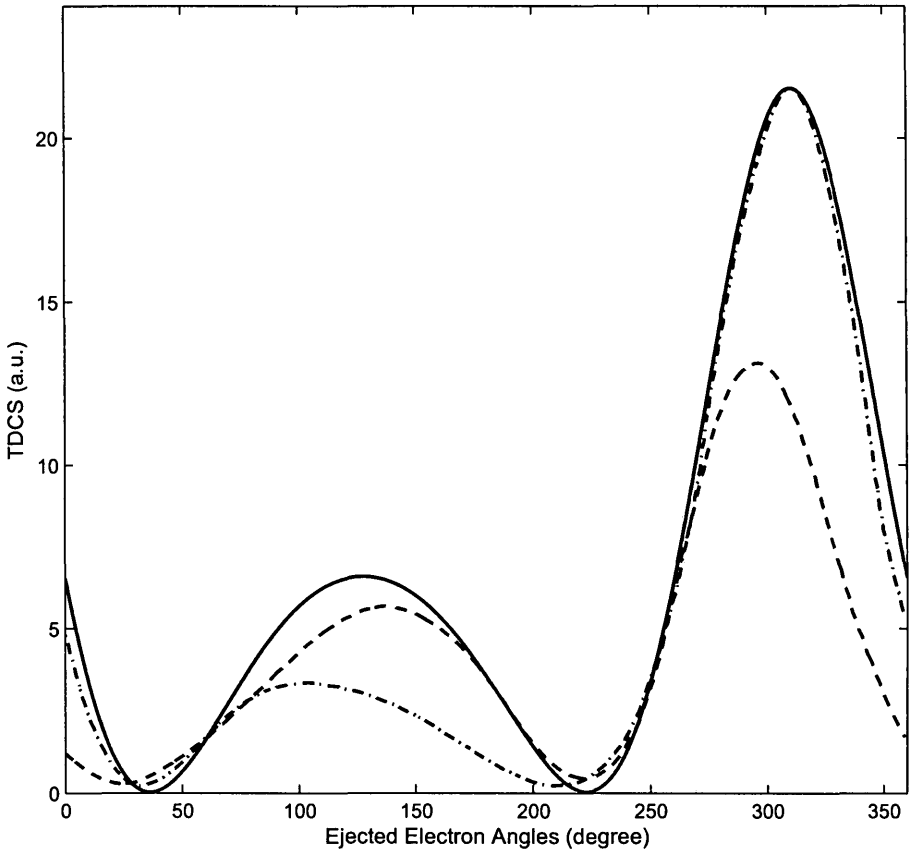

Figure 4.5: Angular dependent TDCS ($a.u.$) in coplanar asymmetric geometry at $E_i = 250\ eV$ positron impact energy, $E_e = 4.5\ eV$ ejection electron energy and $\theta_f = 4°$ scattering angle. Our DWBA-WM model is represented by the solid curve, the 3C electron impact of Stia et al. [7] by the dashed curve and the 3C positron impact of Benedek et al. [8] by the dotted-dash curve. The direction of the momentum transfer vector is at $\mathbf{q} = 123°$ and $(\mathbf{q} + 180°) = 303°$. Our data was divided by a factor of 26.3.

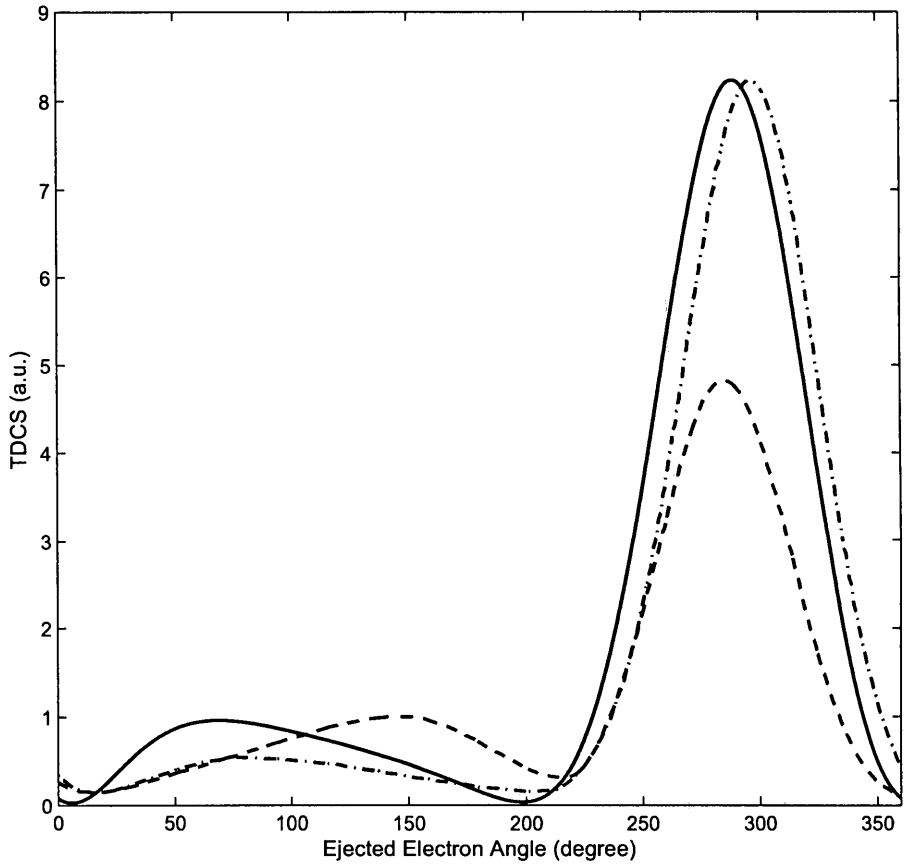

Figure 4.6: Angular dependent TDCS ($a.u.$) in coplanar asymmetric geometry at $E_i = 250\ eV$ positron impact energy, $E_e = 4.5\ eV$ ejection electron energy and $\theta_f = 8°$ scattering angle. Our DWBA-WM model is represented by the solid curve, the 3C electron impact of Stia et al. [7] by the dashed curve and the 3C positron impact of Benedek et al. [8] by the dotted-dash curve. The direction of the momentum transfer vector is at $\mathbf{q} = 110°$ and $(\mathbf{q} + 180°) = 290°$. Our data was divided by a factor of 26.3.

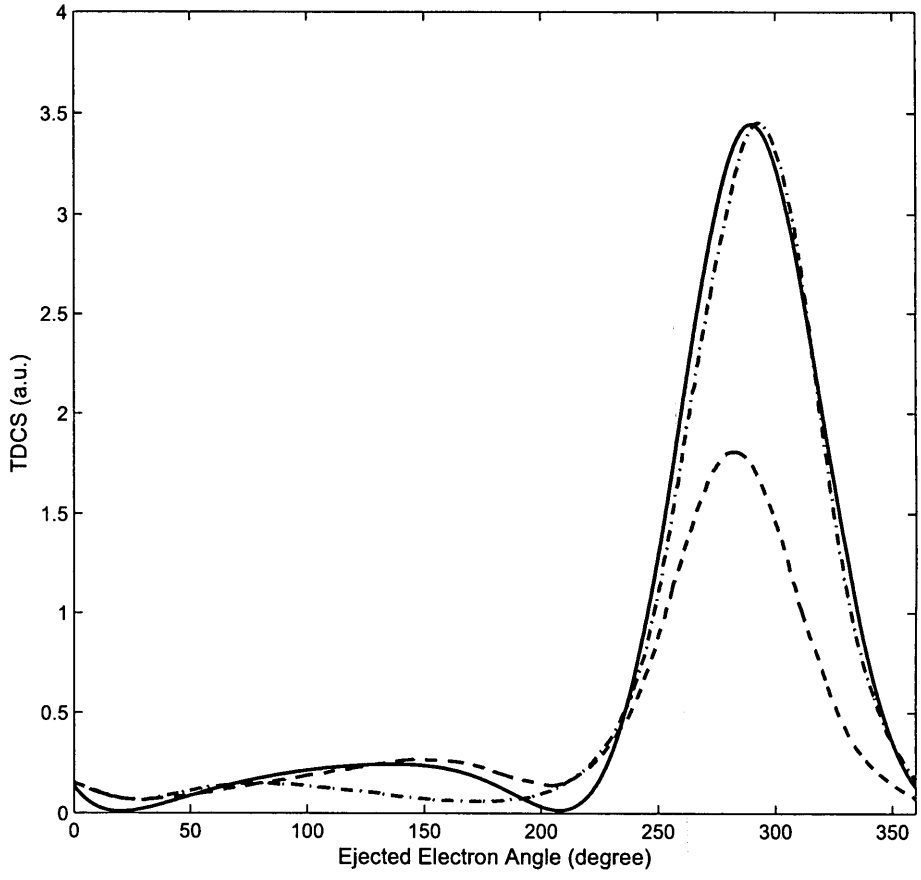

Figure 4.7: Angular dependent TDCS ($a.u.$) in coplanar asymmetric geometry at $E_i = 250\ eV$ positron impact energy, $E_e = 4.5\ eV$ ejection electron energy and $\theta_f = 12°$ scattering angle. Our DWBA-WM model is represented by the solid curve, the 3C electron impact of Stia et al. [7] by the dashed curve and the 3C positron impact of Benedek et al. [8] by the dotted-dash curve. The direction of the momentum transfer vector is at $\mathbf{q} = 107°$ and $(\mathbf{q} + 180°) = 287°$. Our data was divided by a factor of 26.3.

5 Conclusion

In this work we performed an extended study of triple differential cross sections for positron impact ionization of molecular hydrogen. The objective of our work was accomplished by investigating both the electron capture to the continuum phenomenon and the variation with non-zero scattering angles using DWBA-WM and comparing our TDCS results to the 3C findings.

Our distorted wave Born approximation model using Ward and Macek post collision interaction [26] was applied to the ECC study of molecular hydrogen. We were able to show that in this case our model produces TDCS results in good agreement with the existing experimental data. Our convoluted TDCS results are lower in magnitude as compared to the results of the 3C model of Benedek et al. [6]. Since the experimental data available are on a relative scale, we cannot assess the accuracy of the theoretical TDCS size. Thus, the only possible comparison is on the shape of the experimental TDCS and how TDCS measurements vary as the ejected electron energy changes.

In this study we applied our DWBA-WM model to 50 eV and 100 eV impact energies. We found that at 50 eV, our model is able to produce results in better agreement with experimental measurements as compared to the more complex model of 3C. DWBA-WM was able to produce the ECC peak position in agreement to the ECC experimental peak at 15 eV, while the 3C model of Benedek et al. [6] obtained this peak at a position 1.6 eV higher in ejected electron energies.

Many electron impact studies concluded that DWBA-WM approximation gives results in better agreement with experiments than more elaborate models. For instance, Jones et al. [35] and Madison [27] performed their study using three distorted wave models. The 3DW model is an extensions of the 3C model and contain the full Coulomb interaction in the final state of the system between scattered and ejected electrons. These investigators were able to conclude that in impact ionization where the energy is relatively low, three distorted wave models generally overestimate the interaction yet DWBA-WM produces better results. In the case of 100 eV impact energy, the experimental peak at 43 eV was predicted by all three models including our DWBA-WM. However none of the models considered in this thesis correctly approximates the shape of the TDCS at energies lower than 40 eV.

The variation of the TDCS with non-zero scattering angles using our DWBA-WM model was applied to both impact energies $E_i = 100\ eV$ at scattering angles $\theta_f = 7°$, $15°$ and $E_i = 250\ eV$ at scattering angles $\theta_f = 4°$, $8°$, $12°$. In comparing

the five studies we found that the TDCS values decrease as the scattering angles increase and TDCS values also decreases as the impact energy increases.

There is a large difference between the binary peaks in positron and electron impact. By replacing electron projectiles with positron, the electrostatic attraction between the projectile and the ejected electron increases the probability that the ejected electron escapes into the region of the binary peak. However, we found that both positron models: DWBA-WM and the positron 3C model of Benedek et al. [8] predict similar binary peaks. The major difference between the results of our DWBA-WM model and the positron 3C model is the recoil peak. This is where the double scattering process contributes to the TDCS measurements. The difference between DWBA-WM and 3C models is due to the fact that the two models are different treatments of post collision interaction and our DWBA-WM model uses distorted waves where as the 3C uses Coulomb waves. These two main differences in theory have a bigger impact on the recoil peak. To verify the accuracy of the two positron impact ionization theoretical models, experimental measurements of the TDCS with variation in non-zero scattering angles are required.

Bibliography

[1] A. Kövér and G. Laricchia, Phys. Rev. Let., **80**, 5309 (1998).

[2] A. Kövér, K. Paludan, and G. Laricchia, J. Phys. B: Atom. Molec. Phys., **34**, L219 (2001).

[3] A. Kövér and G. Laricchia, Meas. Sci. Technol., **12**, 1875 (2001).

[4] C. Arcidiacono, A. Kövér, and G. Laricchia, Phys. Rev. Let., **95**, 223202 (2005).

[5] J. Fiol, V. Rodrguez, and R. Barrachina, J. Phys. B: Atom. Molec. Phys., **34**, 933 (2001).

[6] A. Benedek and R. Campeanu, J. Phys. B: Atom. Molec. Phys., **40**, 1589 (2007).

[7] C. Stia et al., Phys. Rev. A, **66**, 052709 (2002).

[8] A. Benedek and R. Campeanu, Nucl. Instr. Meth. Phys. Res. B, **266**, 458 (2008).

[9] A. Prideaux and D. Madison, Phys. Rev. A, **67**, 052710 (2003).

[10] R. Campeanu, Nucl. Instr. Meth. Phys. Res. B, **276**, 30 (2012).

[11] M. Rødbro and F. Andersen, J. Phys. B: Atom. Molec. Phys., **12**, 2883 (1979).

[12] A. Kövér, R. Finch, G. Laricchia, and M. Charlton, J. Phys. B: Atom. Molec. Phys., **30**, L507 (1997).

[13] D. Schultz and C. Reinhold, J. Phys. B: Atom. Molec. Phys., **23**, L9 (1990).

[14] D. Madison and O. Al-Hagan, J. Phys. B: Atom. Molec. Phys., **2010**, 367180 (2010).

[15] M. Brauner, J. Briggs, and H. Klar, J. Phys. B: Atom. Molec. Phys., **22**, 2265 (1989).

[16] M. Abramowitz and I. Stegun, *Handbook of Mathematical Functions*, Dover Publications, New York, United States of America, 1972.

[17] A. Nordsieck, Phys. Rev., **93**, 785 (1954).

[18] A. Benedek, *Triple Differential Cross Section Calculations For The Ionization Of Molecular Hydrogen And Helium By Positron Impact*, PhD thesis, York University, 2007.

[19] A. S. Kheifets, A. Naja, E. M. S. Casagrande, and A. Lahmam-Bennani, J.Phys. B: Atom. Molec. Phys., **41**, 145201 (2008).

[20] L. Nagy and L. Végh, Phys. Rev. A, **46**, 284 (1992).

[21] I. Levine, *Quantum Chemistry*, Prentice Hall, New Jersey, United States, 2000.

[22] D. Varshalovich, A. Moskalev, and V. Khersonskii, *Quantum Theory of Angular Momentum*, World Scientific, Philadelphia, United States, 1st edition, 1988.

[23] S. Wang, Phys. Rev., **31**, 579 (1928).

[24] R. I. Campeanu, J. W. Darewych, and A. D. Stauffer, J.Phys. B: Atom. Molec. Phys., **30**, 5033 (1997).

[25] J. Botero and J. Macek, Phys. Rev. Lett, **68**, 576 (1992).

[26] S. J. Ward and J. H. Macek, Phys. Rev. A, **49**, 1049 (1994).

[27] O. Al-Hagan, C. Kaiser, D. Madison, and A. J. Murray, Nat Phys **5**, 59 (2009).

[28] R. Campeanu, personal communication, 2013.

[29] R. Walpole, R. Myers, S. Myers, and K. Ye, *Probability and Statistics for Engineers and Scientists*, Prentice Hall, Boston, United States, 9 edition, 2012.

[30] F. Olver, D. Lozier, R. Boisvert, and C. Clark, *NIST Handbook of Mathematical Functions*, Cambridge University Press, Cambridge, United Kingdom, 2010.

[31] K. Jung, E. Schubert, D. Paul, and H. Ehrhardt, J. Phys. B: Atom. Molec. Phys., **8**, 1330 (1975).

[32] J. Berakdar, Phys. Rev. Let., **81**, 1393 (1998).

[33] H. Klar, A. Roy, P. Schlemmer, K. Jung, and H. Ehrhardt, J. Phys. B: Atom. Molec. Phys., **20**, 821 (1987).

[34] M. Schulz, R. Moshammer, A. Perumal, and J. Ullrich, J. Phys. B: Atom. Molec. Phys., **35**, L161 (2002).

[35] S. Jones, D. Madison, A. Franz, and P. Altick, Phys. Rev. A, **48**, R22 (1993).